IUST
Iran University of Science and Technology

Iranian Journal of Electrical and Electronic Engineering

Journal Homepage: ijeee.iust.ac.ir

Research Paper

Study on Generation of Higher Order Orbital Angular Momentum Modes and Parameters Affecting the Vortex

S. Singh*, M. D. Upadhayay*(C.A.), and S. Pal**

Abstract: In this manuscript, higher-order Orbital Angular Momentum (OAM) modes and parameters affecting vortex in the radiation pattern have been studied. A uniform circular array resonating at 10 GHz frequency is formed using eight identical rectangular patch antennas. Three uniform circular arrays are analyzed, simulated, and fabricated for OAM modes 0, +1, and -1 respectively. The higher-order OAM modes ±2, ±3, and ±4 are simulated and their effects on radiation and phase pattern are discussed. The effect of number of antenna elements and radius of the circular array on the phase purity of higher order OAM modes is presented. The results of simulated radiation patterns and phase front are well satisfying the generation of OAM modes. The measured results show a close agreement with the simulated result.

Keywords: Orbital Angular Momentum, Phase Pattern, Vortex, Power Phase Divider Network.

1 Introduction

REQUIREMENT of a high data rate is increasing day by day, especially in mobile communication due to an exponential increase in the number of smartphone users. Due to limited spectrum and polarization states, high-density adaptive coding and channel sharing techniques have been developed for achieving high data rates and increased channel capacity. Still, the demand is partially met. Recently a well-known concept of optical and quantum physics, orbital angular momentum has been experimentally introduced in microwave frequency to enhance the spectrum efficiency and channel capacity by multiplexing of orthogonal OAM modes [1-3]. OAM modes of the propagating EM wave refer to the twisting degree of the helical phase front [4].

Electromagnetic waves carry two types of momentum- linear momentum (LM) and angular momentum (AM). The angular momentum of the EM wave is composed of two contributions: the Spin Angular Momentum (SAM) 'S' and the Orbital Angular Momentum (OAM) 'L'. SAM of EM wave is related to field polarization and commonly characterized in right-handed circular polarization (RHCP) and left-handed circular polarization (LHCP) [5, 6]. While OAM depends on the phase of entire field distribution over the azimuth plane. Which describes a helical/twisted phase front and the degree of twisted wavefront defines the OAM mode number ***l*** and these twisted signals can cram much more data into a single stream. In other words, the OAM wave is providing the extra degree of freedom without increasing the bandwidth [7].

Numerical explanation for developing the OAM attributes using an antenna array in the radio beam is well presented in 2007 by Thidé *et al*. [8]. Later, in 2012, Tamburini *et al*. demonstrated an experiment on simultaneous transmission of the two different OAM modes [3]. This work attracted the interest of researchers to generate OAM beam in microwave region. There are several techniques proposed by researchers to generate OAM beam in radio waves, such as spiral phase plate (SPP) [9-14], holographic diffraction gratings [15, 16], dielectric resonator antenna [17, 18], Complex fabrication technique like meta-surfaces [19, 20], time switched array (TSA) [21], and

Iranian Journal of Electrical and Electronic Engineering, 2021.
Paper first received 09 March 2020, revised 26 August 2020, and accepted 06 September 2020.
* The authors are with the Electrical Engineering Department, Shiv Nadar University, India.
E-mails: ss523@snu.edu.in and madhur_deo@yahoo.com.
* The author is with the Electronics and Communication Engineering, Birla Institute of Technology, Mesra, India.
E-mail: spal@bitmesra.ac.in.
Corresponding Author: M. D. Upadhayay.
https://doi.org/10.22068/IJEEE.17.2.1822

phased uniform circular antenna (UCA) array [22, 26]. TSA required very complex electronic circuitry to produce required time delay whereas phased UCA array is one of the simplest ways to produce $\pm l^{th}$ order OAM mode with N number of antenna elements, because it is easy to fabricate with printed circuit board (PCB) and required no electronic circuitry. Due to the vortex (intensity null) in boreside direction of OAM wave, its reception was always a challenging task, to address this, in February 2020 a distributed antennas scheme for OAM wave in long distance transmission is proposed [26].

The proposed work is an effort to design three compact UCA array for OAM mode l = 0, -1, and +1 respectively and to analyze different OAM properties like, vortex characteristic and OAM phase purity in its totality by changing the design parameters like number of antenna elements (N) used in UCA array, radius of UCA array (R) and higher order OAM mode number l = ±2, ±3, and ±4. The paper is structured as follows: In Section 2 brief theory, supporting mathematical analysis with MATLAB simulations are presented. In Section 3 design of basic patch antenna is discussed. Section 4 is based on design of three OAM antennas for mode 0, -1, and +1 respectively. Further, Section 5 consist of a discussion on simulated and measured results and effects of number of antenna elements and radius of UCA on the vortex of OAM antenna. Finally, conclusions are drawn in Section 6.

2 Theory And Analysis Of Oam Wave

If an electromagnetic field is located within a volume V, then its total linear momentum can be calculated as: $P^{EM} = \int \varepsilon \left(\bar{E} \times \bar{B}\right) dV$. Where ε, $\bar{E}$ and $\bar{B}$ are permittivity, electric field, and magnetic field respectively. The integrand can be interpreted as a density of electromagnetic momentum, known as linear momentum density $\bar{P} = \varepsilon \left(\bar{E} \times \bar{B}\right)$. Similarly, angular momentum is also related to the pointing vector and the energy flux of the electromagnetic field. The total angular momentum of an electromagnetic field contained in a volume is [5, 27]:

$$J^{EM} = \int \left(\bar{r} - \bar{r}_0\right) \times \varepsilon \left(\bar{E} \times \bar{B}\right) dV .$$

The angular momentum density J is defined as: $J\left(r_0\right) = \left(\bar{r} - \bar{r}_0\right) \times \varepsilon \left(\bar{E} \times \bar{B}\right)$. For the origin $\bar{r}_0 = 0$ and $\bar{r}$ is general observation point. From a practical point of view, the angular momentum is a quantity associated with rotational dynamics. Angular-momentum density J is related to the linear-momentum density P, through $\bar{J} = r \times P$ [5, 27].

Based on the above discussion, a circular array of linearly polarized patch antennas, which are placed at a uniform distance to each other and each patch antenna element is fed with a signal of equal magnitude and increasing or decreasing the electrical phase shift of $2\pi l/N$ radian to generate the OAM wave. Increment or decrement in phase depends on the sign of the OAM mode number l. The largest possible OAM mode number (l_{max}) that can be generated by an antenna array of N number of elements is $-N/2 < l_{max} < N/2$. The electrical field vector $\mathbf{E}(\mathbf{r})$ at an observation point $P(r, \theta, \phi')$ can be given by [4, 5].

$$\begin{aligned} \mathbf{E}(\mathbf{r}) &= -\mathbf{J} \frac{\mu_0 \boldsymbol{\omega}}{4\pi} \sum_{n=1}^{N} e^{il\varphi_n} \int \frac{e^{-i\mathbf{k}|\mathbf{r}-\mathbf{r}'|}}{|\mathbf{r}-\mathbf{r}'_n|} dV_n' \\ &\approx -\mathbf{J} \frac{\mu_0 \boldsymbol{\omega} L}{4\pi} \frac{e^{-i\mathbf{k}\mathbf{r}}}{\mathbf{r}} \sum_{n=1}^{N} e^{i(\mathbf{k}.\mathbf{r}'+l\varphi_n)} \end{aligned} \quad (1)$$

where $\mathbf{J}$ is the constant current density vector of the identical patch antenna elements, L is the electric length of the patch element, μ_0 is the magnetic permeability in the vacuum, and $\boldsymbol{\omega}$ and $\mathbf{k}$ are the angular frequency and wave vector, respectively. $\varphi_n = 2\pi n/N$ is the angle of the n^{th} array element position where n = 1, 2, …, N. 'R' is the radius of the array, and N is the total number of antenna elements present in the array. The distance between spatial locations of each element to the observation point P is given by:

$$\mathbf{r}'_n = R \sin\theta \cos\left(\phi' - \phi_n\right) \quad (2)$$

To obtain the behavior of the phase distribution of the field over azimuth plane for different OAM mode number l, the phase component in (3) must be stationary, i.e.

$$k.r + l.\varphi = \text{constant} \quad (3)$$

As per (3), phase front variation of the electric field for different OAM modes over the distance of 2λ along the propagation are calculated (through MATLAB program) and shown in Fig. 1.

3 Basic Planner Antenna

A circular array antenna consisting of eight numbers of inset fed antenna elements that resonate at 10 GHz is designed through CST full-wave electromagnetic simulator. The schematic of an antenna element is shown in Fig. 2(a). FR-4 is used as substrate material with the relative permittivity of ε_r = 4.3, loss tangent = 0.025, and substrate height h = 1.6 mm. The basic antenna element has a length and width of l_p = 6.7 mm and w_p = 6.2 mm respectively. Inset feed length is f_l = 3 mm and the notch gap is n_g = 0.2 mm. The frequency-dependent $|S_{11}|$ characteristic is shown in Fig. 3(d). Inset feed line width is f_w = 0.7 mm, which chosen to correspond to the 100-Ohm impedance line. It is very common to use the 50-Ohm line as inset feed but the use of a 100-Ohm line reduces the complexity of the phase divider circuit. The width of the patch antenna is optimally reduced for the overall compactness of the

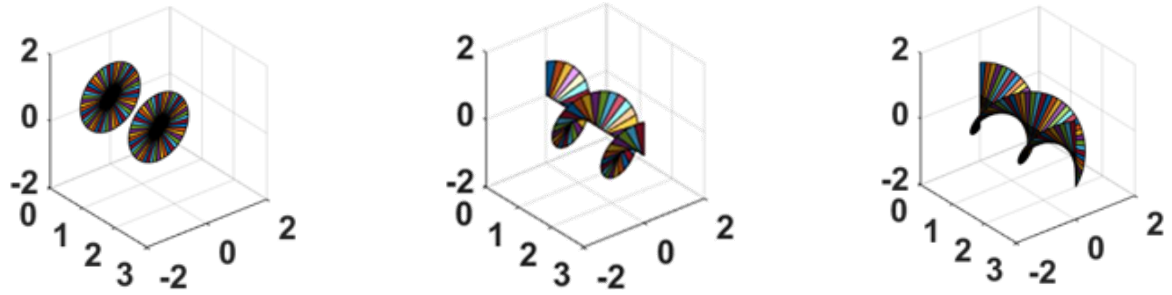

(a) (b) (c)

Fig. 1 Perspective view of analyzed phase front variation over 2λ: a) OAM mode = 0 (Plane wave), b) OAM mode = 1 (Single helical Phase front), and c) OAM mode = 2 (Double helical Phase front).

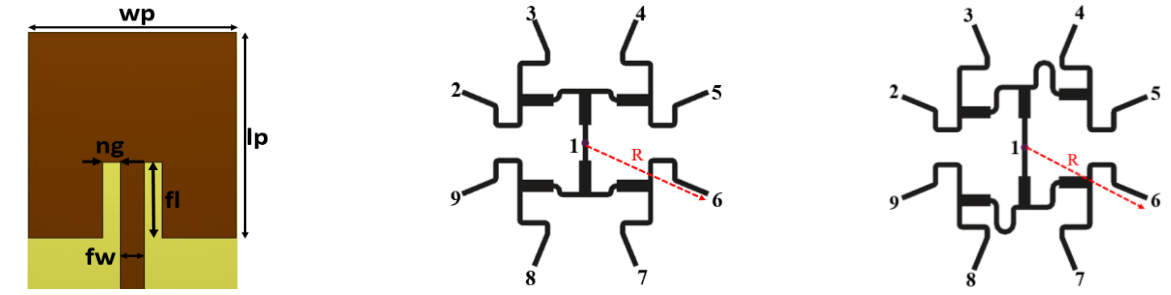

(a) (b) (c)

(d) (e) (f)

Fig. 2 Schematic of : a) antenna element, b) phase divider network for OAM mode '0', and c) phase divider network for OAM mode '-1' phase shifter; Fabricated OAM antenna with N = 8, R = 16 mm for: d) mode l = 0, e) mode l = -1, and f) mode l = +1.

array and reduction of mutual interference between the patch elements.

4 OAM Antenna Structure for Three Different Modes

Antenna structures for OAM modes 0, -1, and +1 are designed by using the microstrip phase-shifted power divider network. The fabricated structures with phase divider network for OAM mode 0, -1, and +1 are shown in Fig. 2.

Phase divider network for +1 mode is a mirror image of -1 mode along the Y-axis, hence it is not shown in Fig. 2 to save the space. At the center of UCA a 50-Ohm coaxial feed is connected as port (1) and eight output ports (2 to 9) of network are used to connect the eight antenna elements. For the generation of OAM wave, an electrical phase shift of $2\pi l/N$ radian is maintained, because OAM mode number l depends on the progressive phase shift between each successive antenna. The microstrip feeding networks with a progressive phase shift of 0°, –45°, and 45° are designed for achieving OAM mode 0, mode -1, and mode +1 respectively and the results of successive electrical phase difference are shown in Figs. 3(a) and 3(b). The requisite electrical phase shifts are achieved by varying the physical length in terms of guided wavelength in microstrip structure. To get 45° relative electrical phase difference between two consecutive paths, the required difference in physical length must be $\lambda_g/8$.

Requisite electrical phase shifts are achieved by varying the physical length in terms of guided wavelength in microstrip structure. To get 45° relative electrical phase difference between two consecutive paths, the required difference in physical length must be $\lambda_g/8$. All antenna elements are fed with the same phase at 10 GHz for generation of OAM mode 0 and the results are shown in Fig. 3(a). For generation of mode number -1, progressive electrical phase of –45° between successive antenna elements is given at 10 GHz. It is observed that the orientation of n^{th} and $(n+4)^{th}$ (keeping n = 1 to 4) antenna elements are opposite to each other, which creates the radiating field opposite to each other (180^0

out of phase) so the physical length of feed line for OAM mode -1 for n^{th} and $(n+4)^{th}$ antenna elements is kept same as depicted in Fig. 2. Hence, phase plots of four cases are shown in Fig. 3(b). For generation of mode +1, the electrical phase between successive antenna elements is kept +45° degrees at 10 GHz. Phase divider network for OAM mode +1 is a mirror image of OAM mode -1 along the Y-axis which makes the relative phase leading in nature. Impedance transformer of characteristics impedance 70.7 Ohm and quarter wavelength 4.2 mm is used for improvement in impedance bandwidth.

To minimize the radiation side lobes and to reduce inter-element mutual coupling, the radius 'R' of circular array plays an important role. Increase in the radius results reduction in inter-element mutual coupling. This occurs due to the increment in inter element spacing. After many iterations, an optimal radius is taken to be 0.53 times of free space wavelength and corresponding to this radius inter-element mutual coupling is found to be below -25 dB, as shown in Fig. 3(c). Inter-element mutual coupling is found to be responsible for frequency deviation from its center frequency as shown in Fig. 3(d).

5 Results and Discussions

The simulated transmission phase of 0° phase divider network is shown in Fig. 3(a) when input is applied to port 1 (located at the center of UCA) and outputs are observed at port 2 to 9 (at the feed points of all patch antenna elements). The simulated result clearly shows almost 0° phase difference at 10 GHz. Fig. 3(b) shows -45° phase difference at 10 GHz for –45° phase divider network that is used to achieve –45° progressive phase shift for –1 OAM mode antenna. Similarly +45° progressive phase divider network is designed to generate +1 OAM mode. This network is mirror image of –45° phase divider network, therefore results are not shown. The simulated mutual coupling (transmission coefficients) due to spatial placement of eight antenna elements for UCA radius R = 16 mm is shown in Fig. 3(c). Measured and simulated return losses of OAM mode 0, –1, and +1 arrays are shown in Fig. 3(d). These results are found to be nearly similar, but having a small shift in frequency. The shift in frequency may be because of fabrication tolerance and/or impedance mismatch of antenna elements with the phase divider network due to inter-element mutual coupling.

The measured $|S_{11}|$ of proposed antenna at 10 GHz frequency for OAM modes 0, -1, and +1 are -14.9 dB, -10.04 dB, and -14.5 dB respectively, which are in good agreement with the simulated $|S_{11}|$ for the same modes that are -18.9 dB, 10.3 dB, and -11.7 dB respectively at 10 GHz, shown in Fig. 3(d). Simulated radiation patterns of single antenna element and eight elements antenna arrays (for modes 0, +1, +2, +3, and +4) are shown in Fig. 4(a). Single antenna element has the main lobe magnitude of 6.21 dBi, along 0° elevation angle,

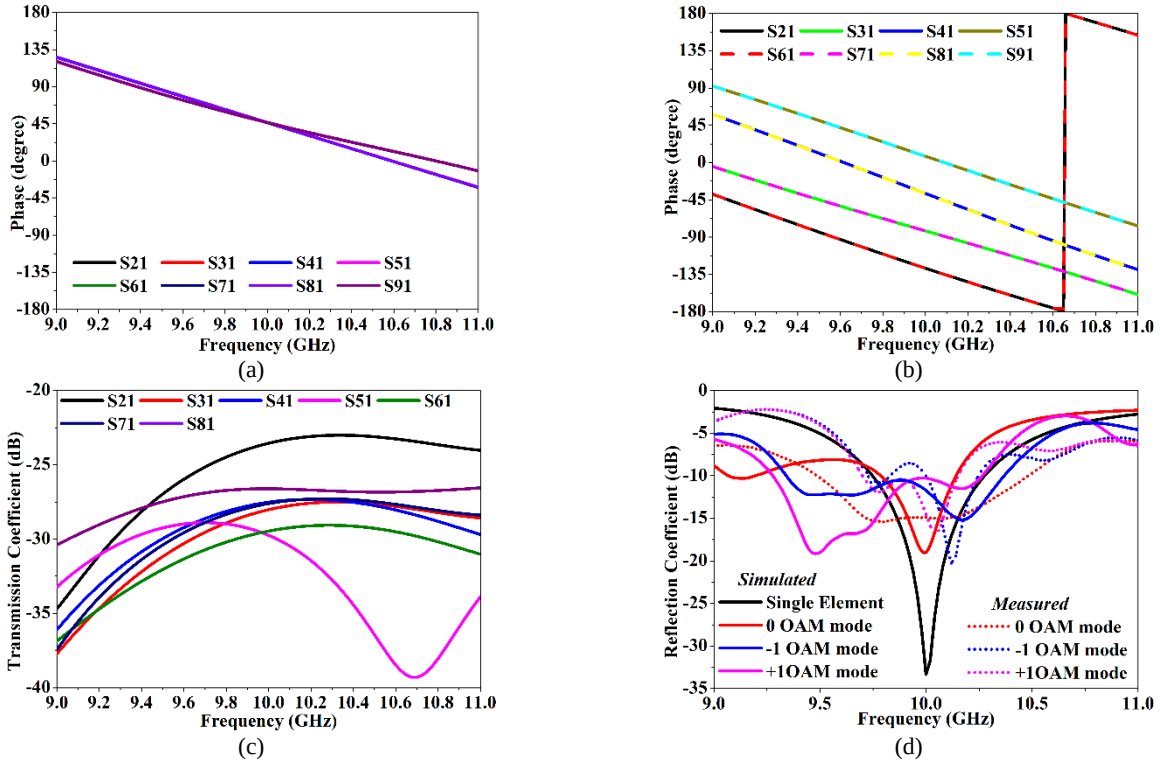

Fig. 3 a) Simulated Phase shift between ports for OAM mode 0, b) Simulated phase shift between ports for OAM mode -1, c) Simulated transmission coefficient (mutual coupling) between each antenna element for R = 16 mm. d) Measured and simulated S_{11} of N = 8, R = 16 mm antenna array for OAM mode 0, -1, and +1.

3dB angular beam width of 95.1° and side-lobe level of -15.7 dB.

It is interesting to note that antenna array (for mode 0, +1, +2, +3, and +4) has vortex along 0^0 elevation angle while the single antenna element has the main lobe in the same direction. Vortex occurs in bore side direction as electric fields cancel each other in this direction. It is also observed from Fig. 4(a) that as OAM mode number l increases from 0 to +4 the angular width of vortex null increases and the main lobe magnitude decreases.

The main lobe of 0 to +4 OAM mode antennas have magnitudes of 9.6 dBi, 9.532 dBi, 6.33 dBi, 6.15 dBi, and 4.84 dBi, respectively. The main lobe direction of OAM mode 0 antennas is in 23° and 337° elevation angle. The -10 dB point is observed at approximately 4.4° and 355.6°, so the -10 dB vortex null-width is 8.8°. In the case of OAM mode +1 the main lobe direction is in 23° and 337° elevation angle. The -10 dB point is observed at approximately 4.6° and 355.4°, so the -10 dB vortex null-width is 9.2°. For OAM mode +2 the main lobe direction is in 23° and 337° elevation angle. The -10 dB point is observed at approximately 4.8° and 355.2°, so the -10 dB vortex null-width is 9.6°. For OAM mode +3 the main lobe direction is in is in 36° and 324° elevation angle. The -10 dB point is observed at approximately 12.6° and347.4°, so the -10 dB vortex null-width is 25.2°. For OAM mode +4, the main lobe direction is in 53° and 307° elevation angle. The -10 dB point is observed at approximately 23.2° and 336.8°,

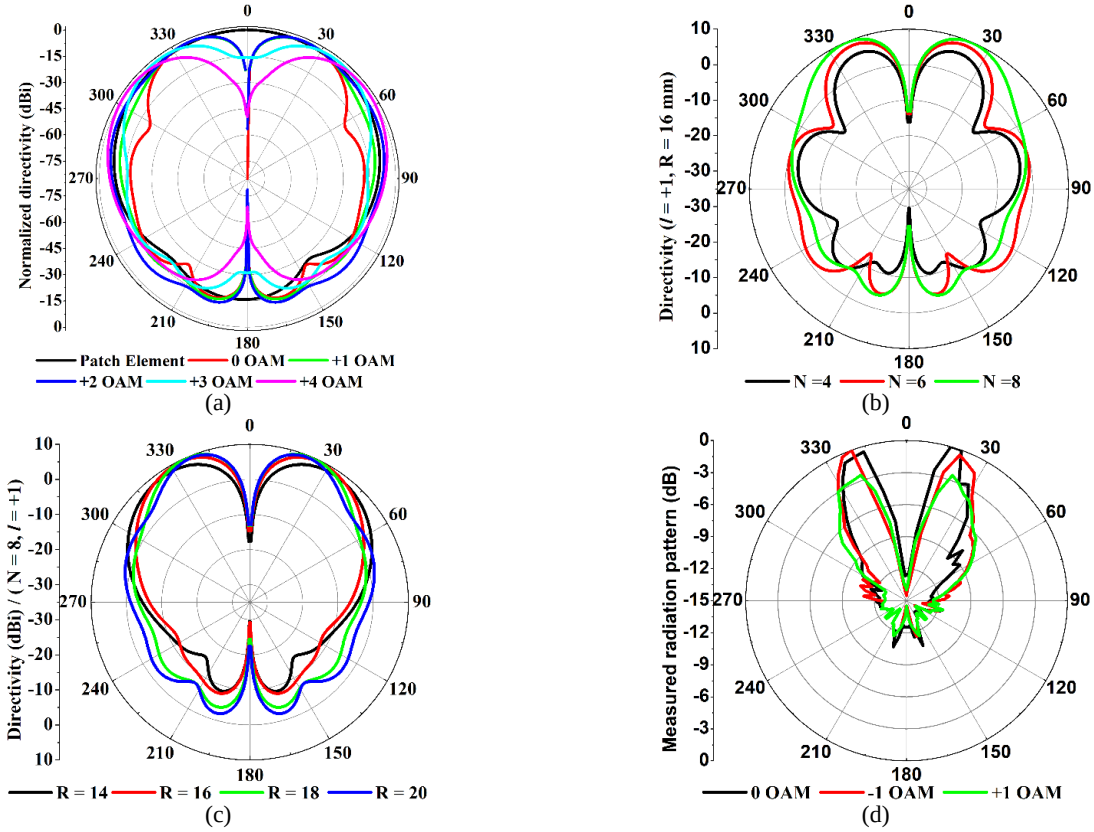

Fig. 4 Radiation pattern: a) Simulated antenna element, eight element OAM array mode 0, +1, +2,+3, and +4 for array radius R = 16 mm, b) Simulated for N = 4, 6, and 8 keeping l = +1 and R = 16 mm, c) Simulated for R = 14, 16, 18, and 20 keeping N = 8 and l = +1, and d) Measured radiation pattern for eight element OAM mode 0, -1, and +1 antenna array.

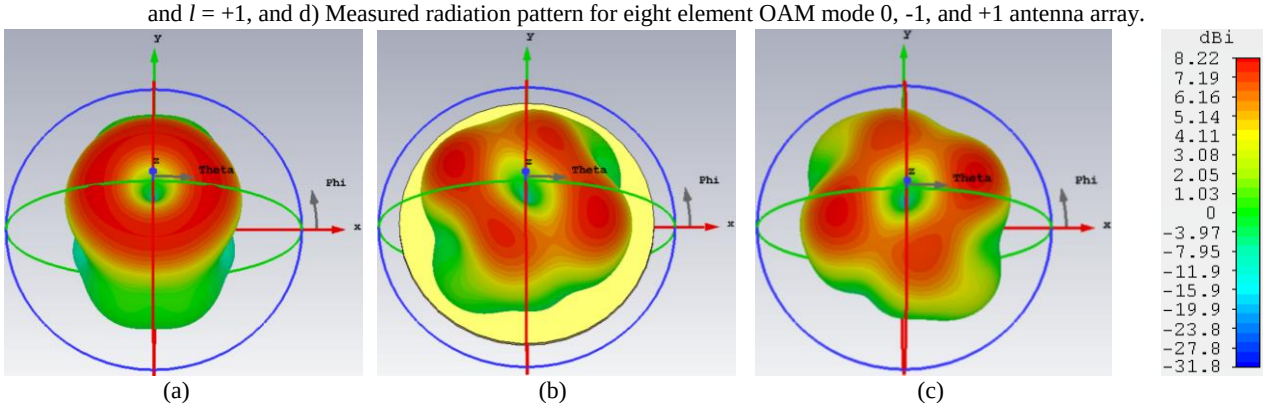

(a) (b) (c)

Fig. 5 Simulated 3D radiation pattern of eight element OAM antenna of: a) mode 0, b) mode +1, and c) mode -1.

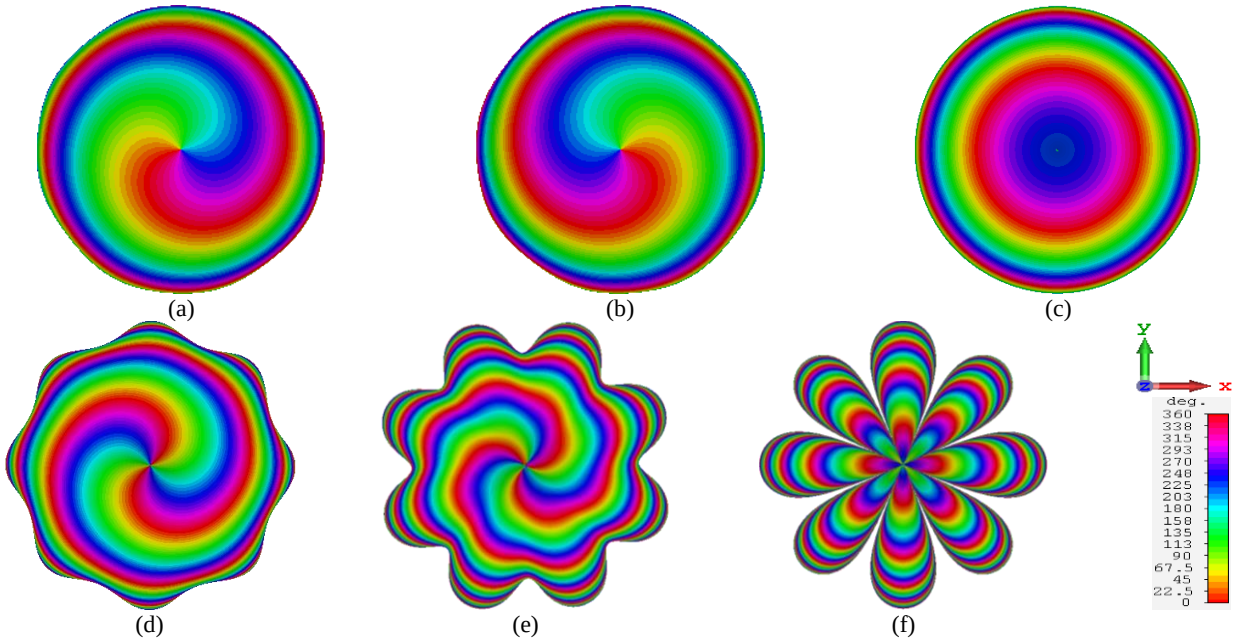

Fig. 6 Simulated 3D phase pattern of eight element OAM antenna of: a) mode +1, b) mode -1, c) mode 0, d) mode +2, e) mode +3, and f) mode +4.

therefore the -10 dB vortex null-width is 46.4°.

Vortex formation occurs due to the cancellation of fields from opposite antenna elements and the amount of field cancellation in bore-side direction (0^0 elevation angle) is represented as vortex-depth, which shows the amount of field cancellation. The vortex-depth for OAM mode 0 to +4 is -85dB, -88 dB, -56 dB, -15.7 dB, -49.5 dB, respectively. Keeping the limit $-N/2 < l_{max} < N/2$, the radiation pattern for mode 0, ±1, ±2, ±3, and ±4 is simulated. It is observed that the radiation patterns for OAM modes -1, -2, -3, and -4 are identical to the modes +1, +2, +3, and +4 respectively. For an OAM mode number l, the angular width of the vortex and radiation pattern does not change with the ± sign of any OAM mode number ($\pm l$), only the direction of phase rotation changes with ± sign of mode number as shown in Fig. 6.

By keeping the radius of antenna array constant (R = 16 mm) for any particular OAM mode (here OAM mode l = +1 is shown) and varying the number of antenna elements (N = 4, 6, 8) in UCA, the radiation pattern for each case is observed and results are shown in Fig. 4(b). This is observed that as the number of antenna elements 'N' increases, the null-width of the vortex and antenna gain increases. In the case of four element UCA (N = 4) the main lobes are in the direction of 20° and 340° elevation angle with the absolute directivity of 5.725 dBi. The -10 dB point is observed at approximately 4° and 356°, so the -10 dB vortex beam-width is 8° and vortex-depth along bore-side is -81.2 dB. In case of six element UCA (N = 6) the main lobe direction is in 21° and 339° with the absolute directivity of 8.408 dBi. The -10 dB point is observed at 4.2° and 355.8°, so the -10 dB vortex beam-width is 8.4° and vortex-depth along bore-side is -86 dB. In the case of eight element UCA (N = 8) the main lobe direction is in 23° and 337° with the absolute directivity of 9.826 dBi. The -10 dB point is observed at 4.5° and 355.5° approximately, hence the -10 dB vortex beam-width is 9° and vortex-depth along bore-side is -87.3 dB.

The array radius (R) is varied from 14 mm to 20 mm in step of 2 mm and keeping the number of antenna elements N = 8 and mode l = +1 constant. This results that as array radius R increases the angular width of the vortex decreases as shown in Fig. 4(c). For R = 14 mm, the main lobe direction is in 34° and 326° elevation angle with the absolute directivity of 8.457 dBi. The -10 dB point is observed at approximately 6.8° and 353.2°, so the -10 dB vortex null-width is 13.6° and vortex-depth along bore-side direction is -77.3 dB. For R = 16 mm, the main lobe direction is in is in 27° and 333° elevation angle with the absolute directivity of 9.516 dBi. The -10 dB point is observed at approximately 5.2° and 354.8°, so the -10 dB vortex null-width is 10.4° and vortex-depth along bore-side direction is -77.5 dB. For R = 18 mm, the main lobe direction is in 23° and 337° elevation angle with the absolute directivity of 9.826 dBi. The -10 dB point is observed at approximately 4.8° and 355.2°, so the -10 dB vortex null-width is 9.6° and vortex-depth along bore-side direction is -87.3 dB. For R = 20 mm, the main lobe direction is in 22° and 338° elevation angle with the absolute directivity of 9.399 dBi. The -10 dB point is observed at approximately 4.5° and 355.5°, so the -10 dB vortex null-width is 9° and vortex-depth along bore-side direction is -78.1 dB.

The measured radiation pattern (normalized) of all three fabricated antennas are shown in Fig. 4(d). These

radiation patterns also have vortex along the bore side. Measured radiation patterns are obtained to be closely matching with the simulated patterns, as shown in Fig. 5. Simulated 3D phase pattern for OAM modes +1, –1, 0, +2, +3, and +4 are shown in Fig. 6. The rotating phase front of the wave supports the OAM concept and the rotation direction is clockwise and counter-clockwise for the negative mode number and positive mode number respectively. These rotating phase fronts are very similar to the numerically obtain phase front from (4) (Fig. 1). From the simulation of the phase front for mode ±4 (Fig. 6(f)), the conclusion has been drawn that, as the mode number increases beyond the limit $-N/2 < l_{max} < N/2$ ($-4 < l_{max} < 4$), the purity of the OAM phase decreases. Higher order mode number has a higher progressive phase shift $\Delta\varphi l$ as $\varphi l = 2\pi l/N$ (here $N = 8$), hence differential phase shift increases as shown in Table 1.

OAM antenna has the rotating phase front in both near field and far field. The distance between AUT and reference antenna is kept greater than $2D^2/\lambda$ for far field, where D is the largest dimension of the test antenna and λ is free space wavelength. The proposed miniaturized antenna array has circular geometry with diameter 10.35 mm, so the far field distance must be more than 39.4 mm. The phase of all three OAM antenna is measured in 2D square plane (test plane) parallel to the aperture of the transmitting OAM antenna (test antenna). A monopole antenna is connected with vector network analyzer (VNA) through phase-stable cable and is used as probe to detect the phase at 20 cm away from the test antenna. The orientation of the probe antenna is kept parallel to the aperture of the test antenna. The size of test plane is 10 cm×10 cm and 400 phase samples are recorded through VNA, by moving the probe in the test plane in steps of 5 mm along both in X and Y-plane. These recorded phases are processed and plotted in MatLab to obtain the phase distributions. This phase measurement procedure is carried out for OAM antenna of modes –1 and 1. The measured results are shown in Fig. 7, which exhibits the same trend as simulated result as shown in Fig. 6. The aperture of receiver antenna should be larger than the aperture of OAM antenna, due to presence of the vortex in the center of OAM antenna.

The comparison with the two similar kinds of reported work is shown in Table 2. This clearly shows, the proposed three OAM antenna designs have single layered compact structure and can generate more than two modes relative to other reported OAM antennas. Our work gives the detailed insight of vortex depth and vortex null for different OAM modes; for various array radius; and for different number of antenna elements.

Table 1 Mode number and progressive phase shift (in radian) in eight element OAM antenna.

l_{φ_n}	φ_0 0	φ_1 π/4	φ_2 π/2	φ_3 3π/4	φ_4 π	φ_5 5π/4	φ_6 6π/4	φ_7 7π/4	$\Delta\varphi = \varphi_n - \varphi_{n-1}$
$l = 0$	0	0	0	0	0	0	0	0	0
$l = 1$	0	0.79	1.57	2.36	3.14	3.93	4.71	5.50	0.79
$l = 2$	0	1.57	3.14	4.71	6.28	7.85	9.43	11.00	1.57
$l = 3$	0	2.36	4.71	7.07	9.43	11.78	14.14	16.49	2.36
$l = 4$	0	3.14	6.28	9.43	12.57	15.71	18.85	21.99	3.14
$l = 5$	0	3.93	7.86	11.78	15.71	19.64	23.56	27.49	3.93
$l = 6$	0	4.71	9.43	14.14	18.85	23.56	28.27	32.99	4.71
$l = 7$	0	5.50	11.00	16.49	21.99	27.49	32.99	38.49	5.50
$l = 8$	0	6.28	12.57	18.85	25.13	31.42	37.70	43.98	6.28

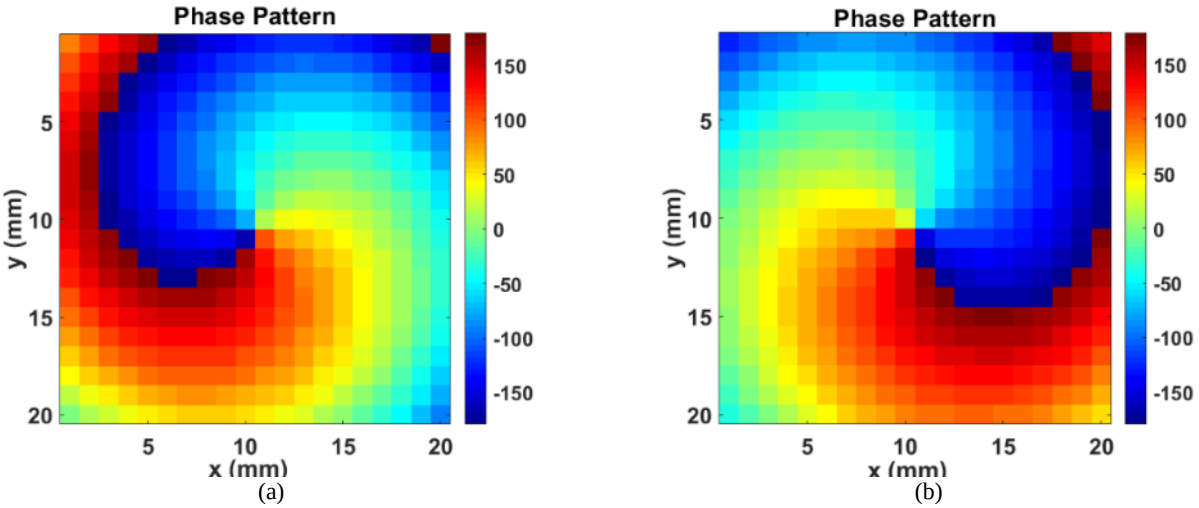

(a) (b)

Fig. 7 Measured phase front of eight element OAM antenna array at 10 GHz of on a square plane (100 mm×100 mm) at a distance of 200 mm; a) mode +1 and b) mode -1.

Table 2 Comparison of different parameters.

Parameters	Ref. [22]	Ref. [23]	This work
Array radius	18 mm	80.59 mm	16 mm
No. of elements	8	8	8
Array elements orientation	Linear, (along Y axis)	Radial	Radial
Antenna designed for modes	+1, -1	+1, -1	+1, 0, -1
Feed line design for modes	+1, -1	+1, -1	+1, 0, -1
Effect of array radius	Not discussed	Not discussed	Discussed
Effect of number of antenna element	Not discussed	Not discussed	Discussed
Structure of antenna	Single layer	Multi-layer	Single layer
Vortex-depth and vortex null-width of different OAM mode	Not discussed	Not discussed	Discussed
OAM modes with single antenna	One	Two	One

Further, we demonstrated the study on phase purity for higher order OAM modes.

6 Conclusion

OAM antennas for different modes have been designed, fabricated, and tested. Parametric variation for all modes has been studied and taken into consideration for designing such a novel OAM antenna structure without sacrificing the purity of OAM mode. The proposed uniform circular radial element array has a radius of 16 mm. Hence, it is compact among reported OAM antenna at 10 GHz.

Three OAM antenna arrays have been designed with specific feed networks for OAM mode 0, –1, and +1. Simulated and measured results show that the designed circular arrays have the property of the generating OAM beam. The result of the simulated antenna array for OAM mode ±2 and ±3 has been discussed. This study may be useful in designing a good practical OAM antenna for achieving higher channel capability, especially in MIMO applications.

References

[1] M. P. Lavery, D. J. Robertson, A. Sponselli, J. Courtial, N. K. Steinhoff, G. A. Tyler, A. E. Willner, and M. J. Padgett, "Efficient measurement of an optical orbital angular-momentum spectrum comprising more than 50 states," *New Journal of Physics*, Vol. 15, No. 1, p. 013024, 2013.

[2] J. Wang, J. Y. Yang, I. M. Fazal, N. Ahmed, Y. Yan, H. Huang, Y. Ren, Y. Yue, S. Dolinar, M. Tur, and A. E. Willner, "Terabit free-space data transmission employing orbital angular momentum multiplexing," *Nature Photonics*, Vol. 6, No. 7, pp.488–496, 2012.

[3] F. Tamburini, E. Mari, A. Sponselli, B. Thidé, A. Bianchini, and F. Romanato, "Encoding many channels on the same frequency through radio vorticity: first experimental test," *New Journal of Physics*, Vol. 14, No. 3, p. 033001, 2012.

[4] F. Tamburini, E. Mari, B. Thidé, C. Barbieri, and F. Romanato, "Experimental verification of photon angular momentum and vorticity with radio techniques," *Applied Physics Letters*, Vol. 99, No. 20, p. 204102, 2011.

[5] R. A. Beth, "Mechanical detection and measurement of the angular momentum of light," *Physical Review*, No. 50, Vol. 2, p. 115, 1936.

[6] K. Y. Bliokh, A. Y. Bekshaev, and F. Nori, "Dual electromagnetism: Helicity, spin, momentum and angular momentum," New Journal of Physics, Vol. 15, No. 3, p. 033026, 2013.

[7] S. M. Mohammadi, L. K. Daldorff, J. E. Bergman, R. L. Karlsson, B. Thidé, K. Forozesh, and T. D. Carozzi, "Orbital angular momentum in radio—A system study," *IEEE Transactions on Antennas and Propagation*, Vol. 58, No. 2, pp.565–572, 2010.

[8] B. Thidé, H. Then, J. Sjöholm, K. Palmer, J. Bergman, T. D. Carozzi, Y. N. Istomin, N. H. Ibragimov, and R. Khamitova, "Utilization of photon orbital angular momentum in the low-frequency radio domain," *Physical Review Letters*, Vol. 99, No. 8, p. 087701, 2007.

[9] G. A. Turnbull, D. A. Robertson, G. M. Smith, L. Allen, and M. J. Padgett, "The generation of free-space Laguerre-Gaussian modes at millimetre-wave frequencies by use of a spiral phaseplate," *Optics Communications*, Vol. 12, No. 4–6, pp. 183–188, 1996.

[10] R. Niemiec, C. Brousseau, K. Mahdjoubi, O. Emile, and A. Ménard, "Characterization of an OAM flat-plate antenna in the millimeter frequency band," *IEEE Antennas and Wireless Propagation Letters*, Vol. 13, pp. 1011–1014, 2014.

[11] X. Hui, S. Zheng, Y. Hu, C. Xu, X. Jin, H. Chi, and X. Zhang. "Ultralow reflectivity spiral phase plate for generation of millimeterwave OAM beam," *IEEE Antennas and Wireless Propagation Letters*, Vol. 14, pp. 966–969, 2015.

[12] Y. Yan, G. Xie, M. P. J. Lavery, H. Huang, N. Ahmed, C. Bao, Y. Ren, Y. Cao, L. Li, Z. Zhao, A. F. Molisch, M. Tur, M. J. Padgett, and A. E. Willner. "High-capacity millimetre-wave communications with orbital angular momentum multiplexing," *Nature Communications*, Vol. 5, No. 1, 2014.

[13] Z. Zhao, Y. Yan, L. Li, G. Xie, Y. Ren, N. Ahmed, Z. Wang, C. Liu, A. J. Willner, P. Song, H. Hashemi, H. Yao, D. Macfarlane, R. Henderson, N. Ashrafi, S. Ashrafi, S. Talwar, S. Sajuyigbe, M. Tur, A. F. Molisch, and A. E. Willner. "A dual-channel 60 GHz communications link using patch antenna arrays to generate data-carrying orbital-angular-momentum beams," in *IEEE IEEE International Conference on Communications (ICC)*, pp. 1–6, May 2016.

[14] H. Yao, H. Kumar, T. Ei, S. Sharma, R. Henderson, S. Ashrafi, D. MacFarlane, Z. Zhao, Y. Yan, and A. Willner, "Experimental demonstration of a dual-channel E-band communication link using commercial impulse radios with orbital angular momentum multiplexing," in *IEEE Radio and Wireless Symposium (RWS)*, pp. 51-54, 2017.

[15] S. Chávez-Cerda, M. J. Padgett, I. Allison, G. H. C. New, J. C. Gutiérrez-Vega, A. T. O'Neil, I. MacVicar, and J. Courtial, "Holographic generation and orbital angular momentum of high-order Mathieu beams," *Journal of Optics B: Quantum and Semiclassical Optics*, Vol. 4, No. 2, p. S52, 2002.

[16] F. E. Mahmouli and S. D.Walker, "4-Gbps uncompressed video transmission over a 60-GHz orbital angular momentum wireless channel," *IEEE Wireless Communication Letters*, Vol. 2, No. 2, pp. 223–226, Feb. 2013.

[17] Y. Pan, S. Zheng, J. Zheng, Y. Li, X. Jin, H. Chi, and X. Zhang, "Generation of orbital angular momentum radio waves based on dielectric resonator antenna," *IEEE Antenna and Wireless Propagation Letters*, Vol. 16, pp. 385–388, 2016.

[18] J. Ren, K. W. Leugn, D. Q. Liu, K. M. Luk, and J. F. Mao, "Orbital angular momentum radiator multiplexing electromagnetic waves in free space," *Optics Express*, Vol. 28, No. 1, pp. 345–359, 2020.

[19] S. Yu, L. Li, G. Shi, C. Zhu, and Y. Shi, "Generating multiple orbital angular momentum vortex beams using a metasurface in radio frequency domain," *Applied Physics Letters*, Vol. 108, No. 24, p. 241901, 2016.

[20] M. L. Chen, L. J. Jiang, and E. I. Wei, "Ultrathin complementary metasurface for orbital angular momentum generation at microwave frequencies," *IEEE Transactions on Antenna and Propagation*, Vol. 65, No. 1, pp.396–400, 2017.

[21] A. Tennant and B. Allen, "Generation of OAM radio waves using circular time-switched array antenna," *Electronics Letters*, Vol. 48, No. 21, pp. 1365–1366, 2012.

[22] Q. Bai, A. Tennant, and B. Allen, "Experimental circular phased array for generating OAM radio beams," *Electronics Letters*, Vol. 50, No. 20, pp. 1414–1415, 2014.

[23] Z. G. Guo and G. M. Yang, "Radial uniform circular antenna array for dual-mode OAM communication," *IEEE Antenna and Wireless Propagation Letters*, Vol. 16, 2017.

[24] T. Yuan, Y. Cheng, H. Q. Wang, and Y. Qin, "Generation of OAM radio beams with modified uniform circular array antenna," *Electronics Letters*, Vol. 52, No. 11, pp. 896–898, 2016.

[25] F. Spinello, E. Mari, M. Oldoni, R. A. Ravanelli, C. G. Someda, F. Tamburini, F. Romanato, P. Coassini, and G. Parisi, "Experimental near field OAM-based communication with circular patch array," *arXiv preprint arXiv:1507.06889*, 2015.

[26] Y. Zhao and C. Zhang, "Distributed antennas scheme for orbital angular momentum long distance transmission," *IEEE Antenna and Wireless Propagation Letters*, Vol. 19, No. 2, pp. 332–336, 2020

[27] J. D. Jackson, *Classical Electrodynamics*. Chapter 6, 3rd ed., Wiley, 1999.

S. Singh born in India in 1986. He is Ph.D. scholar at Electrical Engineering Department, Shiv Nadar University, India. He received Bachelor of Engineering (Electronics & Communication) in 2009 from Rajiv Gandhi Proudyogiki Vishwavidhyalya, India, and Master of Technology (Microwave Electronics) in 2011 from University of Delhi South Campus, India. He has worked Assistant Professor at RGPM, Bhopal, India from 2010 to 2011. He has published 02 articles in journals and 04 papers in conferences.

M. D. Upadhayay born in India in 1979. He received Bachelor of Engineering (Electronics & Communication) and Master of Engineering (Microwave Communication and Radar Engineering) from Dr. Bhimrao Ambedkar University Agra, India, in 2002 and 2004, respectively. He earned his Ph.D. (RF & Microwave Engineering) degree from C.A.R.E., Indian Institute of Technology, Delhi, India in 2014. He has worked as a Lecturer from 2004 to 2006. He joined Electrical Engineering Department, Shiv Nadar University, India as Assistant Professor in 2013 and continue as Associate Professor. He has published 14 articles in journals, 56 papers in conferences (majorly IEEE). He is the recipient of CSIR International Travel Grant (2009), DST International Travel Support (2014) and MHRD Govt. of India- Institute Assistantship (2006–2010).

S. Pal born in India. He received Ph.D (Oxford University), M.E. (Jadavpur University), B.Tech. (NIT Warangal) degrees. He has worked as Assistant Professor in IIT Roorkee, India from 2005 to 2006. He joined ECE Department, BIT Mesra, India as Associate Professor in 2008 and he continues as Professor from 2011. He has published 45 articles journals, 31 papers in conferences. He has one patent. He is recipient of Honorary Research Fellow by University of Birmingham, UK (2010 -2014).